The Journal of Physiology

Gating of the designed trimeric/tetrameric voltage-gated H^+ channel

Yuichiro Fujiwara[1], Tatsuki Kurokawa[1], Kohei Takeshita[1,2], Atsushi Nakagawa[2,3], H. Peter Larsson[4] and Yasushi Okamura[1,2,3]

[1] *Integrative Physiology, Department of Physiology, Graduate School of Medicine, Osaka University, Suita, Osaka, Japan*
[2] *Supermolecular Crystallography, Research Center for State-of-the-Art Functional Protein Analysis, Institute for Protein Research, Osaka University, Suita, Osaka, Japan*
[3] *Graduate School of Frontier Biosciences, Osaka University, Suita, Osaka, Japan*
[4] *Department of Physiology and Biophysics, University of Miami Miller School of Medicine, Miami, FL, USA*

Key points

- The voltage-gated H^+ channel assembles as a dimer by the cytoplasmic coiled-coil domain.
- This study focuses on understanding the structural characteristics and functional significance of dimerization.
- Monomeric, trimeric and tetrameric channels can be engineered by changing the assembly state of the coiled coil by mutation, and interestingly, they show functional currents.
- However, only the native dimeric form shows successful cooperative gating, which is of physiological importance in the phagosomal production of reactive oxygen species.
- These results help us to understand better why the native form of the channel is a dimer from a standpoint of molecular structure and physiological function.

Abstract The voltage-gated H^+ channel functions as a dimer, a configuration that is different from standard tetrameric voltage-gated channels. Each channel protomer has its own permeation pathway. The C-terminal coiled-coil domain has been shown to be necessary for both dimerization and cooperative gating in the two channel protomers. Here we report the gating cooperativity in trimeric and tetrameric Hv channels engineered by altering the hydrophobic core sequence of the coiled-coil assembly domain. Trimeric and tetrameric channels exhibited more rapid and less sigmoidal kinetics of activation of H^+ permeation than dimeric channels, suggesting that some channel protomers in trimers and tetramers failed to produce gating cooperativity observed in wild-type dimers. Multimerization of trimer and tetramer channels were confirmed by the biochemical analysis of proteins, including crystallography. These findings indicate that the voltage-gated H^+ channel is optimally designed as a dimeric channel on a solid foundation of the sequence pattern of the coiled-coil core, with efficient cooperative gating that ensures sustained and steep voltage-dependent H^+ conductance in blood cells.

(Received 19 August 2012; accepted after revision 15 November 2012; first published online 19 November 2012)
Corresponding author Y. Fujiwara: Laboratory of Integrative Physiology, Department of Physiology, Graduate School of Medicine, Osaka University, Yamadaoka 2-2, Suita 565-0871, Osaka, Japan. Email: fujiwara@phys2.med.osaka-u.ac.jp

Introduction

Signal transduction across biological membranes is central to life, and H^+ permeation is one of the key regulators of pH homeostasis (Decoursey, 2003). VSOP/Hv1 is a voltage-gated H^+ channel (Hv) that forms a pathway for sustained transmembrane H^+ conduction in phagocytes and spermatozoa (Ramsey *et al.* 2006, 2009; Sasaki *et al.* 2006; Morgan *et al.* 2009; Okochi *et al.* 2009; Lishko *et al.* 2010). VSOP/Hv1 functions as a dimer (Koch *et al.* 2008; Lee *et al.* 2008; Tombola *et al.* 2008), and its assembly is mediated by dimer coiled-coil architecture in the

 DOI: 10.1113/jphysiol.2012.243006

cytoplasmic C-terminus (Li *et al.* 2010; Fujiwara *et al.* 2012). Each channel subunit has its own permeation pathway and behaves as Hv (Koch *et al.* 2008; Tombola *et al.* 2008). This contrasts with other tetrameric voltage-gated channels that form a pore at the centre of the four subunits. Therefore, the functional role of dimer assembly is distinct from formation of the permeation pathway. One characteristic derived from the dimer assembly in the Hv channel is the cooperative gating (Gonzalez *et al.* 2010; Tombola *et al.* 2010; Fujiwara *et al.* 2012). The activation and deactivation kinetics of the wild-type (WT) dimeric channel are ∼10 times slower than those of the monomeric channel. Voltage dependence of activation is two times steeper in the dimeric channel than in the monomeric channel. The gating movement of one channel subunit affects the gating of the other subunit within the dimeric unit (Koch *et al.* 2008; Gonzalez *et al.* 2010; Tombola *et al.* 2010; Fujiwara *et al.* 2012). This sharp voltage dependence of Hv activities helps sustained production of superoxide anion by phagocytic NADPH oxidase, the enzymatic activity of which is voltage sensitive in the mammalian immune system; i.e. the electron transfer via the NADPH oxidase is effectively compensated by H^+ efflux through Hv in a voltage-dependent manner (DeCoursey *et al.* 2003). However, it remains elusive whether the 'dimer' is the only permissive stoichiometry for Hv function. Perhaps, forming the 'trimer' or 'tetramer' might show more effective coupling than the native dimeric channel. Alternatively, forming 'trimer' or 'tetramer' might disturb cooperative gating, altering adequate formation of the interaction interface of protomers in the coiled-coil domain and in the transmembrane domain. Thus, the significance for the 'dimeric' design of the channel remains fully elucidated.

The dimeric assembly of Hv is mediated by the dimer coiled coil in the cytoplasmic C-terminus (Fujiwara *et al.* 2012). It is possible that the oligomeric state of Hv could be modified by changing the oligomeric state of the coiled-coil assembly. There are several studies of the oligomeric state and changes in oligomerization of coiled-coil proteins using a chemically synthesized yeast leucine zipper protein, GCN4, as a standard coiled-coil model (O'Shea *et al.* 1991; Harbury *et al.* 1993, 1994). Our previous high-resolution crystal structure of the coiled-coil domain of mouse VSOP/Hv1 disclosed details of the structural feature of assembly (Fujiwara *et al.* 2012). So far, no attempt has been performed to alter the oligomerization state of full-length Hv protein by introducing mutations into natural coiled-coil segments. These motivated us to explore whether the stoichiometry of Hv could be changed to trimeric or tetrameric channels by altering the coiled-coil structure by amino acid mutation and, if so, what would happen to the functions of these channels with an artificially altered oligomeric state.

Here, we make the trimeric and tetrameric channels by mutating amino acid residues along the hydrophobic core of the coiled-coil domain based on our crystal structure (Fujiwara *et al.* 2012), and compare gating properties with the dimeric channel. By electrophysiological analysis, we find that the slowest gating kinetics are observed in the dimeric channel with remarkable sigmoidicity, while the trimeric and tetrameric channels showed intermediate phenotypes in gating kinetics between the dimer and monomer. We conclude that Hv is optimally designed as a dimeric channel with sustained H^+ conductance with steeper voltage dependence achieved by efficient cooperative gating.

Methods

Cloning and construction design

We used a mouse Hv clone (mVSOP/Hv1) for all experiments in this study (Sasaki *et al.* 2006). DNA corresponding to the mVSOP/Hv1 coiled-coil domain (residues 220–269) was amplified by PCR and ligated into a pET28 (Novagen, Merck KGaA, USA)-derived vector, pET28HMT (Van Petegem *et al.* 2004), kindly given by Dr Daniel L. Minor Jr (UCSF, USA). Designated 'HMT', the vector contained, in sequence, a hexahistidine tag, maltose-binding protein and a cleavage site for the tobacco etch virus (TEV) protease. After subcloning, the sequence around the TEV cleavage site was mutated to obtain an ideal construct encoding a protein that had only one extra residue (Gly) at the N-terminus after the TEV cleavage. The mutants used in the experiments were made by PCR fragment amplification using long primers or by QuikChange protocol (Stratagene Japan, Japan), and all 'a'/'d' positions of the coiled-coil core were changed to I/I, L/L or L/I types. For electrophysiological recordings (Figs 5–7), cDNAs for the mVSOP/Hv1 channel were subcloned into the pIRES-EGFP expression vector (Clontech, Clontech Laboratories, Inc., USA), and mutants were made in the same way.

Protein expression and purification

HMT fusion proteins were expressed in *Escherichia coli* [BL21(DE3)pLysS] grown in 2YT media at 37°C and induced with 0.4 mM IPTG for 4 h. Cells were harvested by centrifugation, and cell pellets were lysed by sonication in lysis buffer (10 mM K_2HPO_4 pH 7.3, 250 mM KCl, 1 mM EDTA, 5 mM β-mercaptoethanol, 1 mM PMSF). The soluble fraction, which contained the HMT fusion protein, was applied to a 20 ml HisPrep FF (GE Healthcare Japan, Japan) nickel-charged column and eluted by 500 mM imidazole on an ÄKTA purifier system (GE Healthcare). The fusion proteins were then applied to a 75 ml amylose (New England Biolabs Japan, Japan) column, and eluted

by 10 mM maltose, after which the maltose was removed on a 53 ml HiPrep desalting column (GE Healthcare). The purified HMT fusion protein was used for the size exclusion chromatogram (Fig. 2). The HMT fusion protein was then cleaved with TEV protease (Kapust *et al.* 2001) (~300 μM for 24 h at 4°C). Coiled-coil proteins were collected in the flow-through from the Hisprep nickel column, and were further purified by the superdex75 gel filtration column (GE Healthcare) for crystallization (Fig. 3). The protein concentration was determined by absorbance (BCA Protein Assay Kit, PIERCE, Pierce Biotechnology Inc., USA).

Size exclusion chromatography

For the isolated HMT-tagged mVSOP/Hv1 coiled coil, 100 μl of 500 μM protein in buffer containing 250 mM KCl and 10 mM Tris (pH 7.3) were passed through a Superdex200 HR 10/30 column (GE Healthcare) equilibrated with the same buffer on an ÄKTA purifier system (GE Healthcare) at 4°C (Fig. 2*A*) (Howard *et al.* 2007; Fujiwara & Minor, 2008). Eluates were monitored at 280 nm over a flow rate of 0.5 ml min^{-1}.

Equilibrium sedimentation

Equilibrium sedimentation experiments were performed at 4°C in a Beckman Optima XL-A analytical ultracentrifuge (Beckman Coulter Japan, Japan) (Fig. 2*B*). The HMT-tagged coiled-coil proteins were dissolved to a concentration of 10 μM in 150 mM KCl and 10 mM K_2HPO_4 (pH 7.3), and the equilibrium distribution was measured based on the absorbance at 292 nm as a function of the radial distance at 7300 rpm for the I/I and L/L mutants and 6000 rpm for the L/I mutant. The molecular mass and residuals for the fittings were calculated as described previously (Laue, 1995; Howard *et al.* 2007).

Crystal structure analysis

The I/I mutant coiled-coil crystals were obtained at 20°C using hanging drop vapour diffusion. The crystals grew from mixtures of 1 μl protein solution (5 mg ml^{-1} protein dissolved in 150 mM KCl and 5 mM Hepes (pH 7.3)) and 1 μl reservoir solution containing 0.2 M $(NH_4)_2SO_4$, 0.1 M Tris-HCl (pH 8.5) and 25% w/v PEG3350. Diffraction data were collected using 20% PEG200 cryoprotectant at BL44XU SPring-8 (Hyogo, Japan) equipped with a MX-225HE CCD detector (Rayonix, USA). The crystals belonged to the $P2_12_12_1$ space group and diffracted X-rays to 2.30 Å. Data were processed using HKL2000 (HKL Research Inc., USA). The primary structure was solved by molecular replacement with Molrep (Vagin & Teplyakov, 2010) using a combination of two trimeric coiled-coil templates (1GCM and 3EFG), and an initial structural model was built using the program Arp/Warp (Perrakis *et al.* 1999). Model building was done in Coot (Emsley *et al.* 2010). The $P2_12_12_1$ space group asymmetric unit contained four trimers, corresponding to 12 α-helices. A resultant model was refined using Phenix (Adams *et al.* 2010) and REFMAC6 (Murshudov *et al.* 1997) (PDB accession code 3VYI) (Fig. 3 and Table 2). The structural comparisons between mVSOP/Hv1 coiled-coil I/I mutant trimer and other coiled coils were carried out using Twister (Strelkov & Burkhard, 2002) and lsqkab in CCP4 suite, and the coiled-coil parameters and the R.M.S. deviations calculated were obtained (Table 3). The structure coordinate for the trimer coiled coil (I/I types) has been deposited in the Protein Data Bank under code 3VYI.

Cross-linking Western blot

HEK293 cells expressing mVSOP/Hv1 WT and mutants were washed with PBS and treated with amine-reactive cross-linker, ethylene glycol bis-(succinimidyl succinate) (EGS). The EGS reaction was quenched with 100 mM Tris-HCl (pH 8.0). Proteins were separated on 12.5% SDS/PAGE under reducing conditions and electrophoretically transferred to Immobilon-P (Millipore, Merck Millipore Japan, Japan). A polyclonal rabbit anti-mVSOP/Hv1 antibody generated against the amino acids Met_1–Ala_{72} in the N-terminus of mVSOP/Hv1 was used for detection (Koch *et al.* 2008; Sakata *et al.* 2010; Fujiwara *et al.* 2012). Horseradish peroxidase-conjugated donkey antirabbit IgG (Amersham Pharmacia Biotech Inc., USA) was used as the secondary antibody. Protein amounts were measured by the CS analyzer system (ver. 3) (ATTO Corporation, Japan) (Fig. 4*B*).

Electrophysiology

The cDNAs for WT and mutant mVSOP/Hv1 channels were transfected into HEK293T cells. The cells were then cultured for 24 h in Dulbecco's modified Eagle's medium supplemented with 10% bovine calf serum. Electrophysiological recordings were carried out 4–16 h after reseeding, which corresponds to 18–30 h after transfection. A coverslip with HEK293T cells was placed in a recording chamber containing bath solution (see below) on the stage of an inverted fluorescence microscope (IX71, Olympus Inc.), and transfected cells were identified by the fluorescent signal from green fluorescent protein. Macroscopic currents were then recorded in the whole cell clamp configuration using an Axopatch-200B amplifier (Molecular Devices, USA). The pipette resistance in the solution was 3–5 MΩ. Sixty to eighty per cent of the voltage error due to the series resistance was compensated by a circuit in the amplifier. The recorded currents were low-pass filtered

at 2 kHz using a four pole Bessel filter circuit built in to the amplifier. The external solution contained 75 mM *N*-methyl-D-glucamine, 1 mM $CaCl_2$, 1 mM $MgCl_2$, 10 mM glucose and 180 mM Hepes (pH 7.0). The pipette solution contained 65 mM *N*-methyl-D-glucamine, 3 mM $MgCl_2$, 1 mM EGTA and 183 mM Hepes (pH 7.0). The recording temperature was controlled at 25°C by adding heated or cold chamber solution to the external solution (Fujiwara *et al.* 2012). Data were analysed using Clampfit (Molecular Devices, USA) and Igor Pro (WaveMetrics, Inc., USA) software. Current densities were calculated by normalizing the current amplitudes by membrane capacitances (Fig. 5*B*). The activation time constant was obtained by fitting the activation phase of the outward currents with a single exponential upon depolarization at 100 mV from the onset of the 1 s step pulse to the

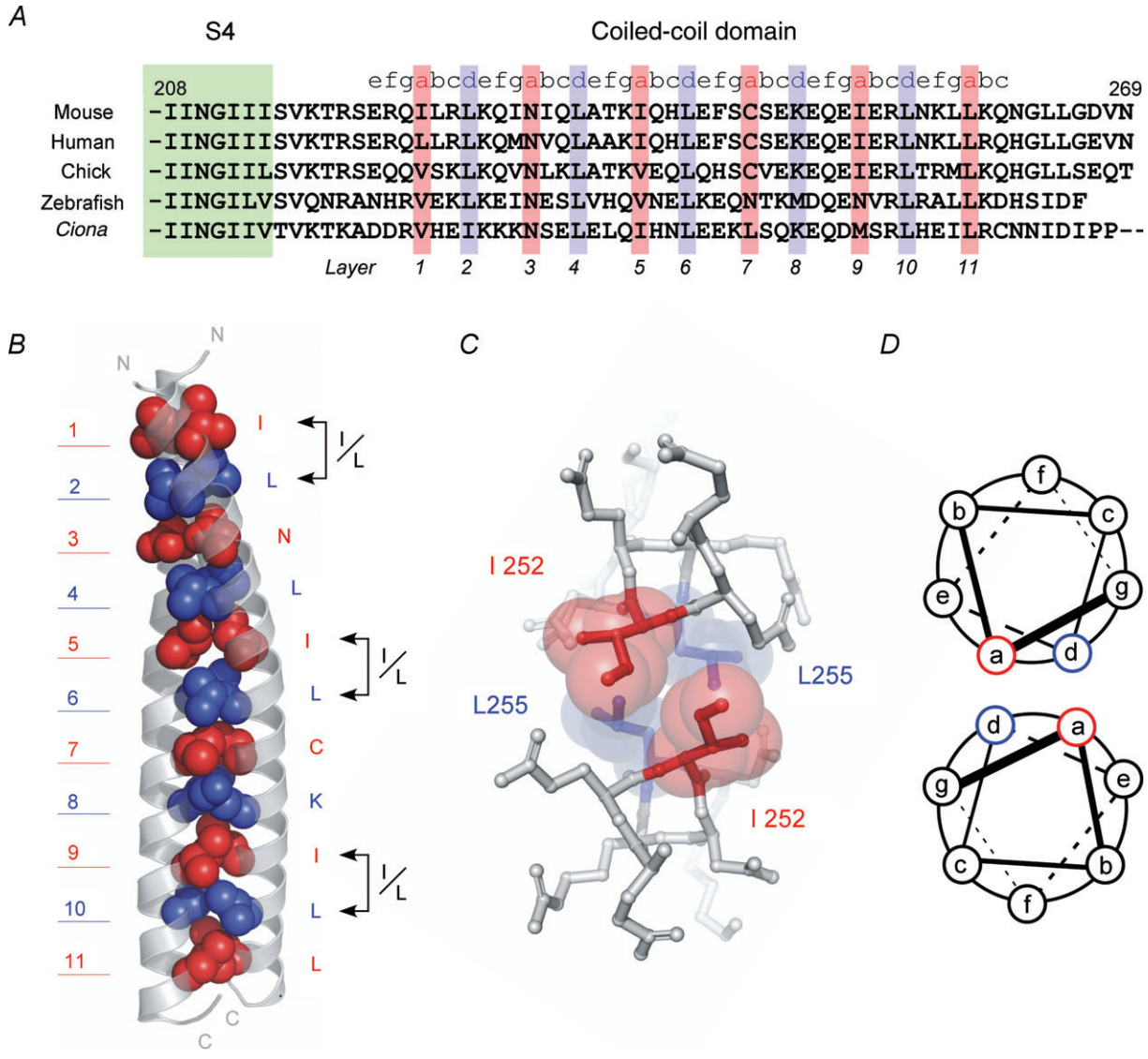

Figure 1. I/L core packing in the Hv Coiled coil domain
A, sequence alignment of the C-terminal cytoplasmic Coiled coil domain from various species of Hv. Coiled-coil residues occupying hydrophobic 'a' and 'd' positions are denoted by blue and red, respectively. Layer positions for each residue in the structure are indicated below the alignment. The green box depicts part of S4. *B*, hydrophobic layers of the coiled-coil core. Van der Waals spheres depicting the side chains of the 'a' (red) and 'd' (blue) layers on a ribbon backbone (grey) are shown. Layer numbers, amino acid residues and the N- and C-termini of the coiled coil are indicated. *C*, representative geometry of the symmetrically packed hydrophobic I/L type coiled-coil core. Highlighted in the hydrophobic core are two Ile residues in layer 9 (red) and two Leu residues in layer 10 (blue). Ball-and-stick representations show each layer of the core. 'a' and 'd' positions are coloured as in (A). *D*, helical wheel representation of the core-packing arrangements found in the homodimeric coiled coil. Heptad repeat positions are labelled *a*–*g*. Core-forming positions are highlighted in colour as in (A), and positions lying in the same layer are linked by solid or dashed lines.

Table 1. Frequency of amino acid residue in the core position

'a'	(%)*	'd'	(%)*	'a'/'d'	(%)*	Twice	(%)†
L	19.8	L	75.4	I/L	1.8	I/L, I/L	0
I	4.2	I	1.2	I/I	0	L/L, L/L	5.9
V	28.7	V	5.4	L/L	13.8	V/L, V/L	26.5
A	7.8	A	0.6	L/I	0	N/L, N/L	23.5
N	26.9	N	0	V/L	21.0	Other	0
Other	12.6	Other	17.4	N/L	25.1	***Thrice***	***(%)***†
				Other	38.3	n/a	0

*Appearance ratio per 167 positions. †Appearance ratio per 34 coiled coils. Appearance frequency of the amino acid residue at positions 'a'/'d' in the human B-ZIP coiled-coil proteins. 34 coiled coils with 167 core positions of 'a'/'d' were used for categorizing. Each B-ZIP has ~10 layers of core positions per a coiled coil, which is almost same to VSOP/Hv1 coiled coils (Fig. 1*A*). L, V and N appears frequently at 'a' position, while the amino acid residues at 'd' are mostly L. L/L, V/L and N/L combinations of the 'a'/'d' core appear frequently, and they sometimes appear twice in a coiled coil. There is no case in which the same 'a'/'d' combination appears three times in a coiled coil (n/a in the 'thrice' column). These probability distributions are considered to be random based on the initial bias of residues at positions 'a' and 'd'.

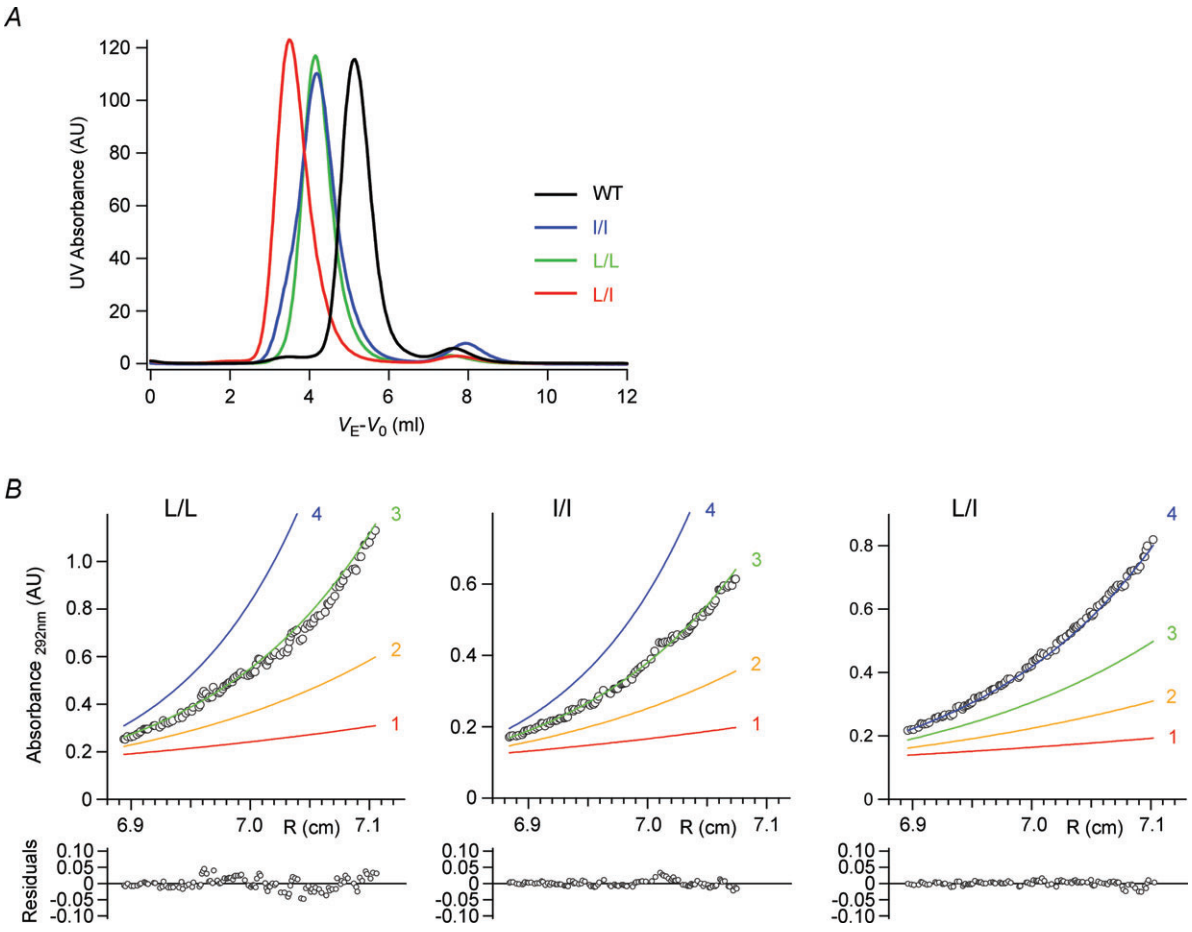

Figure 2. Oligomeric state of the mutant coiled coils
A, coiled-coil stoichiometry determined by Superdex 200 (GE Healthcare) size exclusion chromatography monitored at 280 nm. The elution volume V_E was corrected for the void elution volume by subtracting that of blue dextran (V_0). *B*, sedimentation equilibrium of the coiled-coil proteins. Raw data are shown relative to predicted distribution curves for monomeric (red), dimeric (yellow), trimeric (green) and tetrameric (blue) species. Residuals for each oligomeric distribution are shown below. The oligomeric states were 2.99 ± 0.02 ($n = 3$) in I/I, 2.92 ± 0.01 ($n = 3$) in L/L and 4.04 ± 0.01 ($n = 3$) in L/I. UV, ultraviolet; WT, wild-type; R, radius of rotation.

Table 2. X-ray data collection and refinement statistics

Data collection	I/I trimer
Resolution (A)	50.0–2.30 (2.34–2.30)
Space group	P212121
Cell dimensions: a, b, c (Å)	83.27, 84.01, 88.39
Cell dimensions: α, β, γ (°)	90.00, 90.00, 90.00
R_{sym}	8.9 (44.6)
Wavelength	0.9000
$I/\sigma I$	31.1 (3.9)
Completeness (%)	97.7 (99.1)
Redundancy	6.6 (6.8)
Refinement	
Resolution (Å)	39.1–2.30
No. reflections	27673
R_{work}/R_{free}	23.2 / 28.9
Total protein atoms	4347
Total water atoms	185
Average B factors: protein (Å^2)	46.62
Average B factors: water (Å^2)	44.79
RMSD in bond lengths (Å)	0.01
RMSD in bond angles (°)	0.94

Values in parentheses are for the highest-resolution shell.

pulse end (Fig. 5*C*). In the single exponential fittings, the time gap between the intercept on the *x*-axis and the pulse start was used for measuring the sigmoidicity of activation (Fig. 6). In power–exponential fittings the equation, $I(t) = A(1 - e^{(t/-\tau)})^n + C$, was used. We also used the parallel power–exponential equation, $I(t) = A_1(1 - e^{(t/-\tau 1)})^{n1} + A_2(1-e^{(t/-\tau 2)})^{n2} + C$, for fitting the activation time course to detect extra exponential components (Supplementary Fig. S1). The deactivation time constant was obtained by fitting the tail currents during the hyperpolarization step at −60 mV from 100 mV. The deactivation phase was fitted with a single exponential (Fig. 5*D*) and a double exponential (Fig. 7). Data were analysed statistically, and error bars depict means ± SEM ($n = 6$, 6, 6, 6 and 5 of ΔC, WT, I/I, L/L and L/I, respectively) through all electrophysiological recordings (Fig. 5–7).

Results

Coiled-coil design in a trimer or tetramer

VSOP/Hv1 has four transmembrane domains corresponding to the voltage sensor domain (S1–S4) of other voltage-gated channels. The N- and C-termini of the channel comprise small cytoplasmic domains (Ramsey *et al.* 2006; Sasaki *et al.* 2006). Beginning ∼10 residues C-terminal to the last transmembrane domain (S4), there is a distinctive heptad repeat pattern $(abcdefg)_N$, in which the 'a' and 'd' positions are hydrophobic amino acids (Fig. 1*A*). This repeated pattern is a coiled-coil structure domain. We previously solved a crystal structure of this mVSOP/Hv1 domain and reported that it mediated the dimeric assembly of Hv (Fujiwara *et al.* 2012). The crystal structure of the assembly domain shows a parallel coiled-coil pattern within which the 'a' and 'd' positions form alternate layers along the superhelical core (Fig. 1*B*). It is noteworthy that an I/L core packing pattern, in which Ile/Leu residues are situated at positions 'a'/'d', is periodically observed along the entire length of the coiled coil (layers 1/2, 5/6 and 9/10) (Fig. 1*B*). Frequency of the amino acid residues in the core positions based on human B-ZIP leucine zipper proteins, which are categorized as homodimer coiled coil (Vinson *et al.* 2002), shows that the I/L combination observed in the mVSOP/Hv1 coiled coil is infrequent, and the regular pattern of residues is also unique (Table 1). This I/L pattern was previously reported in the mutated dimer coiled coil of GCN4, a yeast leucine zipper protein (Harbury *et al.* 1993). To examine whether the core-packing pattern can determine the oligomeric state of the mVSOP/Hv1 coiled coil, we mutated the packing pattern to I/I, L/L and L/I types and analysed the molecular weight of the purified proteins of WT and the mutant coiled coils. Size exclusion analysis by gel-filtration chromatogram showed that mutations in the coiled-coil cores shifted the elution peaks toward the direction of higher molecular weight, and they showed clear monodispersity (Fig. 2*A*). Because the molecular weight of elongated proteins, such as coiled coils, has some uncertainty in the size exclusion experiments, we used sedimentation equilibrium experiments to attain a precise measurement of the assembly state of these coiled-coil proteins in solution (Howard *et al.* 2007; Fujiwara & Minor, 2008). Data of the sedimentation analyses of the I/I and L/L mutant coiled coils were well-fitted by a single species model with the molecular mass of a trimer, whereas that of the L/I mutant coiled coil were by a tetramer (Fig. 2*B*). Thus, these data show that the sequence pattern of residues in the hydrophobic core of the coiled coil determined the oligomeric state of the coiled coil part of Hv, and this pattern is in agreement with the GCN4 coiled coil (Harbury *et al.* 1993, 1994).

Crystal structure analysis of I/I trimer coiled coil

Although coiled coils can be readily identified from sequence analysis, their accurate three-dimensional structure, even including their oligomeric state and strand orientation (parallel/antiparallel), is more elusive (Lupas & Gruber, 2005; Grigoryan & Keating, 2008). To categorize the structural feature of the mutant coiled coils, we tried to crystallize the coiled-coil domain constructs with I/I, L/L and L/I patterns. Only the crystals of the I/I mutant coiled coil were obtained. The crystals belonged to the

$P2_12_12_1$ space group and diffracted X-rays to 2.30 Å. We solved the structure by molecular replacement using a combination of two trimeric coiled coils (1GCM and 3EFG) as search models, and the resultant model was refined to an acceptable level ($R/R_{free} = 23.5/28.9\%$) (Table 2). There are four coiled-coil trimers in the asymmetric unit. The overall structure of the I/I mutant coiled coil is that of a parallel left-handed, three-stranded coiled coil. The representative hydrophobic core layer packed in the I/I pattern is indicated (Fig. 3*A*). The side chains of Ile are packed symmetrically into the hydrophobic core, and to be more specific, Cδ1 of Ile participated in the vertical packing; Cδ1 of I245 in the 'a' layer fill the centre space formed by Ile in the 'd' layer, and Cδ1 of I248 in the 'd' layer fill in the space formed by Ile and neighbours in the 'a' layer in the knob-into-hole style (Fig. 3*A*). The I/I mutant coiled coil forms intersubunit hydrogen bond networks in both the N-terminal and the C-terminal ends (Fig. 3*B*). The intersubunit polar contact is reported to stabilize the coiled-coil assembly (Acharya *et al.* 2006; Howard *et al.* 2007). Such interactions are not observed in the native dimeric coiled coil (Fujiwara *et al.* 2012). The structure was compared with parallel three-stranded coiled coils based on the GCN4 leucine zipper peptides and the assembly domains of other channels (Table 3). The data suggest that the I/I mutant coiled-coil trimer is straighter and less twisted than other trimeric coiled coils, in which the GCN4 leucine zipper (I/I type) and the TRPP2 coiled coils are relatively close in shape (Table 3). Thus, the crystal structure shows that the I/I mutant coiled coil forms a well-packed parallel trimer, which is suitable as a cytoplasmic tail just downstream of the last transmembrane segment S4.

Oligomeric state of the full-length channel

We next examined whether the sequence patterns in the hydrophobic core of the coiled coil that determined the oligomeric states of the coiled coils are also applicable

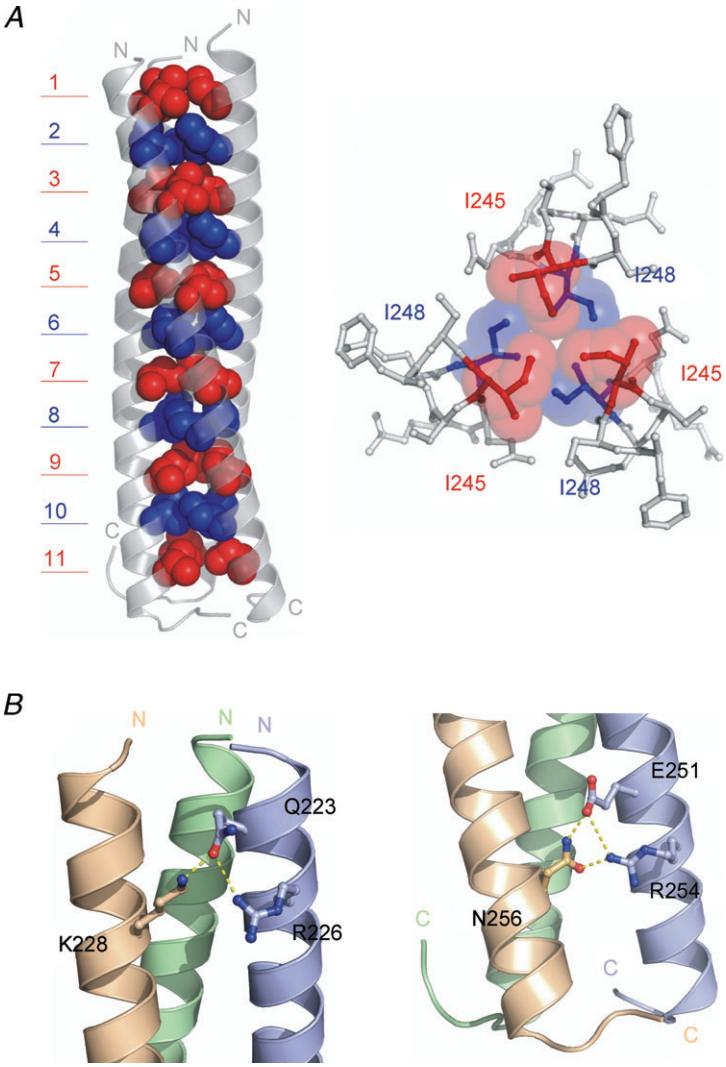

Figure 3. Crystal structure of the I/I mutant coiled coil
A, crystal structure of the I/I mutant coiled-coil hydrophobic layers of the coiled-coil core (left). Representative geometry of the symmetrically packed hydrophobic I/I type coiled-coil core (right). Highlighted in the hydrophobic core are three Ile residues in layer 5 (red) and three Ile residues in layer 6 (blue). Ball-and-stick representations show each layer of the core. 'a' and 'd' positions are coloured as in Fig. 1. *B*, lateral view of the structure of the N-terminal (left) and the C-terminal (right) ends. Intersubunit electrostatic interactions (sticks and yellow dashed lines) are displayed on a ribbon diagram of trimer.

Table 3. Coiled-coil parameters

Analysed range (res. no.)	mVSOP/Hv1 222–261	GCN4_I/I 2–28	GCN4_I/N 2–28	GCN4_V/L 2–28	Kv7.1 trimer 589–607	TRPP2 trimer 836–868	CNGA1 trimer 6–47
Superhelical parameter							
Supercoil radius (Å)	6.56	6.73	6.07	6.35	6.19	6.53	6.81
Residues per superhelix turn	122.9	114.3	109.0	100.6	89.7	110.4	125.8
Supercoil pitch (Å)	180.6	169.1	159.1	147.9	129.2	161.2	184.9
α-Helical parameter							
α-Helix radius (Å)	2.28	2.26	2.28	2.29	2.30	2.28	2.30
Residues per turn	3.61	3.60	3.60	3.61	3.63	3.61	3.64
Rise per residue (Å)	1.51	1.53	1.51	1.52	1.51	1.51	1.51
Radius of curvature (Å)	143.0	118.1	78.24	95.02	87.82	100.97	91.62
RSMD							
vs. mVSOP/Hv1 (Å)	—	0.571	0.784	0.804	0.950	0.715	1.896

Coiled-coil parameters of mVSOP/Hv1 coiled-coil I/I mutant trimer and other trimeric coiled coils. Helical and superhelical parameters obtained by fitting C_α backbone. GCN4_I/I, GCN4_I/N and GCN4_V/L: parallel three-stranded coiled coils based on the GCN4 leucine zipper peptide with the core alignment in I/I, I/N and V/L types (PDB code: 1GCM, 2WQ0 and 1IJ3) (Harbury *et al.* 1993; Akey *et al.* 2001; Hartmann *et al.* 2009). Kv7.1 trimer, TRPP2 trimer and CNGA1 trimer: parallel three-stranded coiled coils from the cytoplasmic domain of ion channels (PDB code: 3HFE, 3HRO and 3SWF) (Xu & Minor, 2009; Yu *et al.* 2009; Shuart *et al.* 2011).

to the assembly machinery of full-length channels. In WT and the mutant types, I/I, L/L and L/I, channels were expressed in HEK293 cells, and their assembling states were analysed by amine-reactive cross-linker, EGS. In this experiment, the data with the saturating amount of cross-linker is most reliable when estimating the oligomeric states (Koch *et al.* 2008; Lee *et al.* 2008), and quantitative analysis of the oligomeric fraction with the maximal dose of EGS (5 mM) was shown (Fig. 4*B*). The protein bands of WT and mutants in the absence of EGS cross-linking (0 mM) were similar, suggesting that protein expressions were little affected by the mutations (Fig. 4*A*). WT showed a strong band as two-fold molecular weight of the monomer (Fig. 4*A* and *B*; orange arrows and bars), as was previously shown (Koch *et al.* 2008; Lee *et al.* 2008; Fujiwara *et al.* 2012). A small amount of tetramer band was also observed in WT in which the channel protein is assumed to make a dimer upon

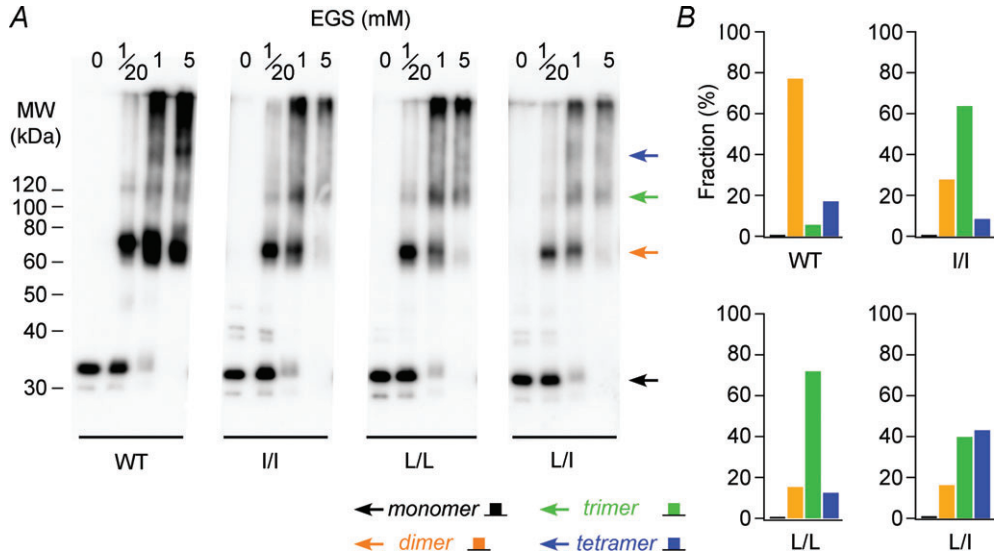

Figure 4. Oligomeric state of the mutant channels
A, oligomeric state of mVSOP/Hv1 channels studied by cross-linker analysis with Western blotting. Wild-type (WT) and the mutant channels (I/I, L/L and L/I) were expressed in HEK293 cells and treated with the indicated concentrations of EGS. Arrows depict the molecular weights (MW) corresponding to one to four oligomeric states. *B*, quantitative analysis of the oligomeric fraction. Data with 5 mM EGS were used. EGS, ethylene glycol bis-(succinimidyl succinate).

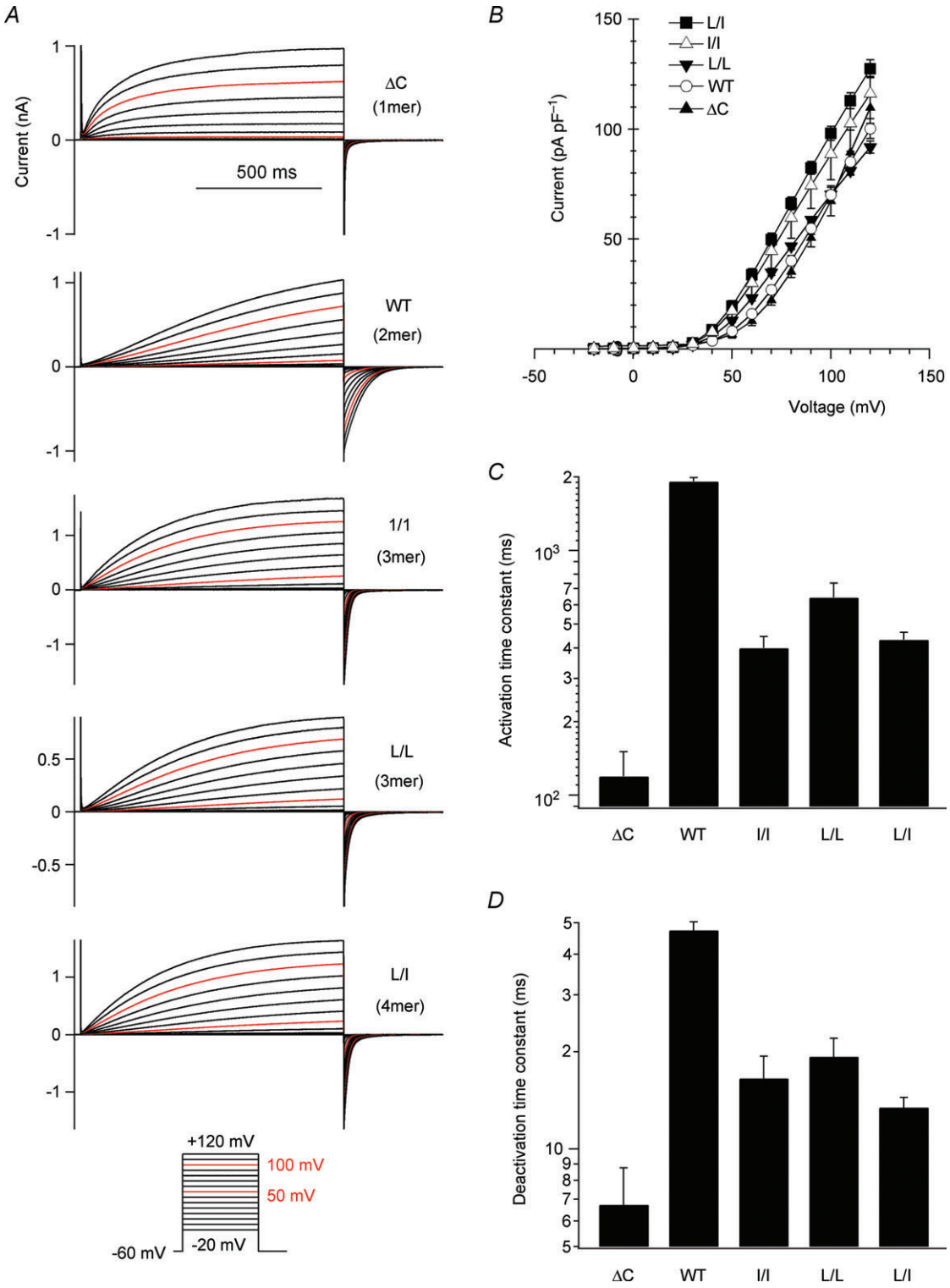

Figure 5. Effect of mutations into the coiled-coil core on the electrophysiological properties
A, representative current traces of the WT and the mutant channels expressed in HEK293T cells. The pulse protocols are indicated in the inset. *B*, current density–voltage relationships at the end of step pulses at 100 mV. Symbols used are in the figure. *C*, the activation phases evoked by the depolarization at +100 mV were fitted with a single exponential function, and the time constants of the fittings are plotted. *D*, the deactivation phases at −60 mV from the +100 mV depolarization step were fitted with a single exponential function, and the time constants of the fittings are plotted. WT, wild-type.

cross-linking. To estimate oligomeric states, we compared signal fractions corresponding to one to four oligomers (Fig. 4*B*). The protein bands from I/I and L/L mutant channels migrated to trimers as a main component with saturating cross-linking by EGS (Fig. 4*A* and *B*; green arrows and bars). In the case of the L/I mutant channel, the protein bands migrated further to the tetrameric molecular weight (Fig. 4*A* and *B*; blue arrows and bars), although the cross-linking seemed incomplete, which is a recognized limitation in amine-reactive cross-linker experiments. We also used disuccinimidyl suberate and glutaraldehyde as cross-linkers, but the cross-linking data for the high molecular weight as a tetramer band were unclear (data not shown). In addition, the mutants, especially L/I, showed the aggregation tendency with cross-linkers, which also makes it difficult to interpret the results. Although the L/I mutant channel may form in multi-oligomeric states, the L/I coiled-coil protein showed a clear tetrameric state with the monodispersity (Fig. 2*A* and *B*), and hence, the L/I mutant channel is assumed to express as a tetramer. Thus, the oligomeric state of the full-length channel assembly is also dominated by the core packing pattern in which the I/L type is a dimer, the I/I and L/L types are trimers and L/I type is presumably the tetramer.

Electrophysiology of the mutant channels

To address how the channel function is affected by assembling states in the trimer or tetramer, we analysed the electrophysiological properties of the I/I, L/L and L/I mutant channels and compare them to those of the dimeric (WT) and monomeric channels. We analysed the ΔC channel as a monomeric channel, in which its C-terminal coiled-coil domain is deleted (Koch *et al.* 2008; Fujiwara *et al.* 2012). The electrophysiological properties of WT and the mutants were analysed by whole cell patch

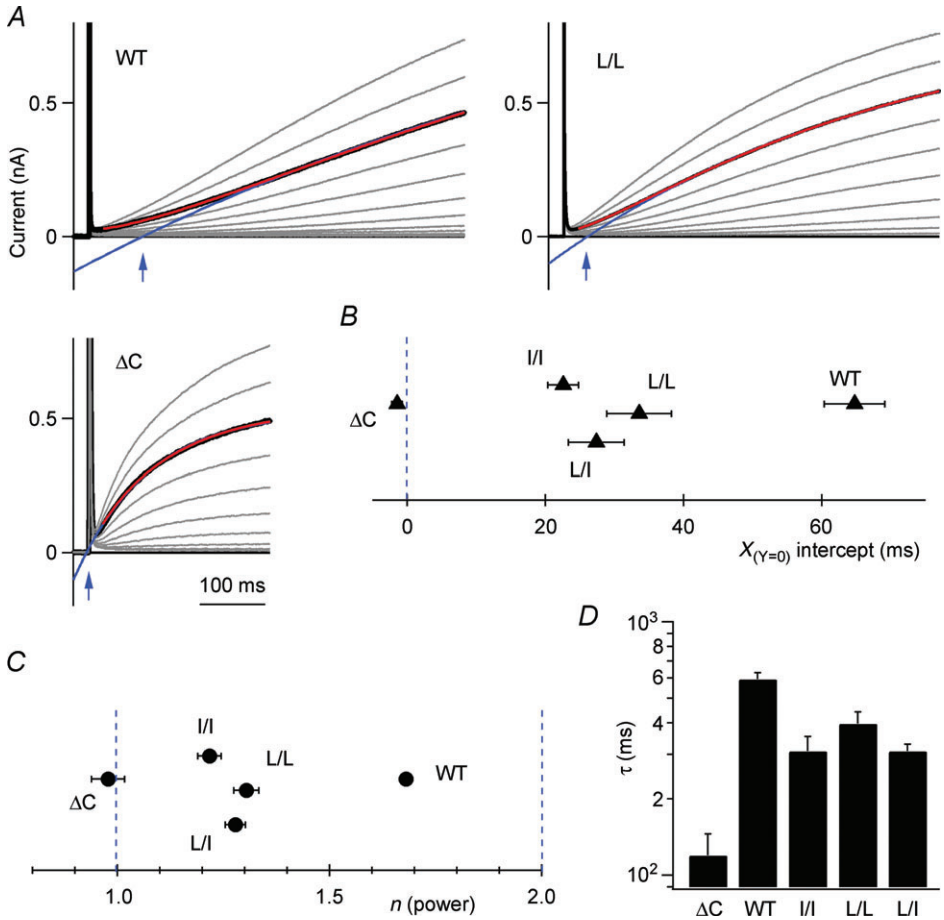

Figure 6. Analysis of the sigmoidal activation phases of the mutant channels
A, enlarged images of the activation phase of the current in the WT, ΔC and L/L mutant channels. Activation phases at +100 mV were fitted by the single exponential equation (blue lines) and by the power-exponential function (red lines) (*B*) $X_{(Y=0)}$ intercepts (blue arrows in *A*) measured from the onset of the step pulse of the single exponential fittings were shown. *C* and *D*, powers, *n*, and kinetics, τ, of the power-exponential fittings were shown, where $I(t) = A(1 - e^{(T/-\tau)})^N + C$ was used. WT, wild-type.

clamp techniques (Fig. 5*A*). Because the gating kinetics are quite dependent on recording temperature (Kuno *et al.* 2009; Fujiwara *et al.* 2012), the recordings were performed strictly at 25°C. Current densities and the activation thresholds of the channel were not changed by mutation (Fig. 5*B*). Both the activation and deactivation kinetics were accelerated by all of the mutations (Fig. 5*A*). The activation and deactivation kinetics were fitted by a single exponential function, and time constants are shown (Fig. 5*C* and *D*). The kinetics of activation and deactivation in the I/I and L/L trimeric channels and L/I channel showed intermediate phenotypes between WT and ΔC (Fig. 5*C* and *D*).

The activation kinetics in Hv WT is not single exponential, but sigmoidal, while that in ΔC is single exponential (Fig. 6*A*). This sigmoidal activation kinetics reportedly reflects the cooperative channel gating within the dimeric unit (Gonzalez *et al.* 2010; Musset *et al.* 2010). The gating of one channel subunit affects the gating of the other subunit, and consequently, the appearance of extra closing states makes the activation phase seem sigmoidal, which is not shown in the ΔC monomeric channel (Gonzalez *et al.* 2010). The degree of sigmoidicity was analysed in two ways. First, the time gap at the intercept on the *x*-axis from the onset of the step pulse was measured when the activation phase was fitted by a single exponential (Fig. 6*B*). In another means of analysing sigmoidicity, the activation phases were fitted by the power-exponential function (Fig. 6*C* and *D*), where the power, *n*, is considered to reflect the gating cooperativity in the two channel protomers. *n* values of I/I, L/L and L/I were 1.2–1.3 larger than that of ΔC (1.0), but smaller than that of WT (1.7). The activation kinetics of I/I, L/L and L/I mutants showed clear but less sigmoidicity (Fig. 6*A*), and the degrees of sigmoidicity were intermediate between WT and ΔC (Fig. 6*B*–*D*). We also used the parallel power-exponential function for fitting to detect the dual components in the activation phase (Supplementary Fig. S1). However, the activation phases were not well-fitted by the simple summation of activation phases of WT and ΔC (Supplementary Fig. S1).

Unlike WT and ΔC, which were best fit by a single exponential, deactivation kinetics of the I/I, L/L and L/I mutants were better fitted by a double exponential function (Figs 5*A* and 7*A*). Two time constants and fractions of the slow component are indicated (Fig. 7*B* and *C*). The deactivation phases of the trimeric and tetrameric channels consist of a fast major and a slow minor component. Taken together, the gating properties of the channel are affected by the oligomeric state of the coiled-coil domain, which is determined by the patterned sequence of the core. The gating kinetics of the trimeric channel showed intermediate phenotypes that consisted of two components.

Discussion

In this study, we introduced series of mutations into hydrophobic residues aligned along the coiled-coil core of mVSOP/Hv1 to change the packing type to I/I, L/L and L/I types. By biochemical analysis the oligomeric states

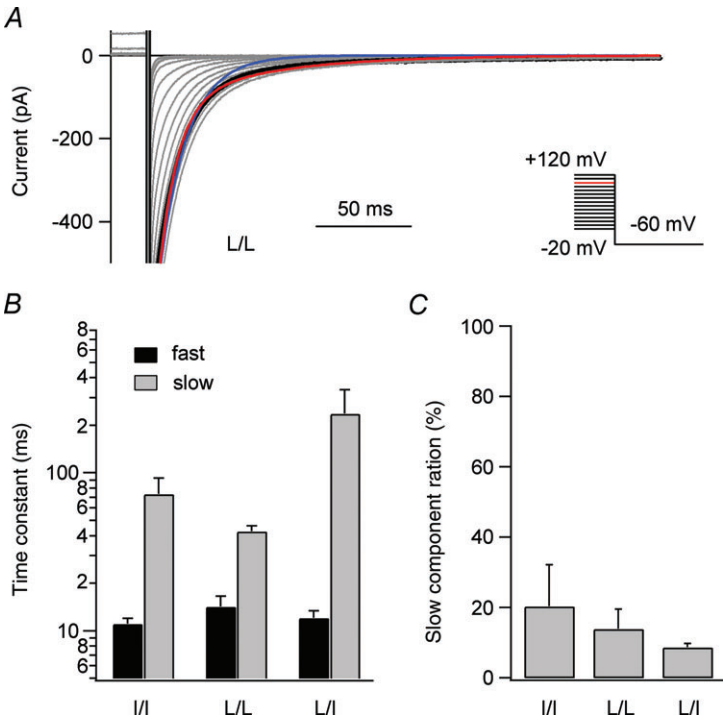

Figure 7. Double exponential kinetics in deactivation of the mutant channels
A, enlarged image of the deactivation phase of the current in the L/L mutant channel. Deactivation phases were fitted by the single exponential equation (blue line). Fittings were much improved by the double exponential equation (red line). *B*, the deactivation phases at −60 mV from the +100 mV depolarization step were fitted with a double exponential function and the Time constants of the fittings are plotted. *C*, content rate of the Slow component in the fitting in (*B*).

of full-length channels were determined by the packing pattern of the hydrophobic core, where the I/I and L/L pattern induced trimers. By electrophysiological analysis of the designed mutant channels, the slowest and most sigmoidal gating kinetics were observed in the dimeric channel, while trimeric channels showed intermediate phenotypes in the gating kinetics between dimer and monomer.

In the coiled-coil structure, hydrophobic residues are wrapped in the centre, 'a' and 'd' positions, by the surrounding hydrophilic residues in 'bcefg' positions (Fig. 1*D*), and therefore the coiled coils are stable in the water-filled environment of the cytoplasm (Alber, 1992). The burial of hydrophobic surfaces, thus, provides the thermodynamic driving force for oligomerization. The packing pattern of the hydrophobic residues for the oligomeric state has been investigated structurally using the GCN4 coiled coil, a yeast leucine zipper, with artificial mutations (Harbury *et al.* 1993). It is noteworthy that the patterned sequence of I/L is intermittently observed along the entire length of the coiled coil of Hv (Fig. 1*B*), and therefore the role of the sequence pattern of the Hv coiled coil is worthy of exploration. The sequence pattern of residues in the hydrophobic coiled-coil core, in this study, determined the oligomeric state of the coiled coil; i.e. the I/I and L/L pattern induced trimers, while the L/I pattern induced tetramers consistent with those in the GCN4 study (O'Shea *et al.* 1991; Harbury *et al.* 1993, 1994). It is further notable that the sequence pattern of the hydrophobic core determined the assembly state in the full-length channel. Hv from different species such as mouse, human and *Ciona* have been determined as dimeric channels (Koch *et al.* 2008; Lee *et al.* 2008; Tombola *et al.* 2008). Despite this, small variations in the amino acid sequence in the hydrophobic core from the I/L type are found in different species (Fig. 1*A*). Val instead of Ile is often situated at position 'a' (Fig. 1*A*, layers 1 and 5). In the crystal structure of mVSOP/Hv1 WT in the position 'a' layer, the Ile–Ile interface consists chiefly of close Cγ1–Cγ1 contact and two separate Cδs hardly contribute to the packing interface of a dimer (Fig. 1*C*). Val has the same structural orientation as Ile up to Cγ1, and this is different from the Leu structure. Hence, Val in position 'a' is assumed to essentially form the same packing in the dimer, which is also supported by observations of the V/L-patterned layer existing in the dimeric coiled-coil structure (O'Shea *et al.* 1991; Harbury *et al.* 1994; Fujiwara *et al.* 2012). Thus, the hydrophobic core packing of the coiled-coil domain in Hv essentially consists of I/L types, which assembles the channels into dimers.

In our trimeric coiled-coil mutants, critical parts for channel gating, such as the transmembrane region and subsequent linking region up to the coiled coil (Tombola *et al.* 2010; Fujiwara *et al.* 2012) remained intact. The success of converting dimeric Hv into a trimeric channel upon alteration of the coiled-coil amino acid sequence in this study confirms our previous view that the C-terminal coiled coil is sufficient to determine dimer assembly of the whole channel protein (Fujiwara *et al.* 2012). In analysing these mutant channels, we attempted to determine the functional significance of dimerization in the gating of Hv. It has been reported that a cooperativity within two channel protomers appears

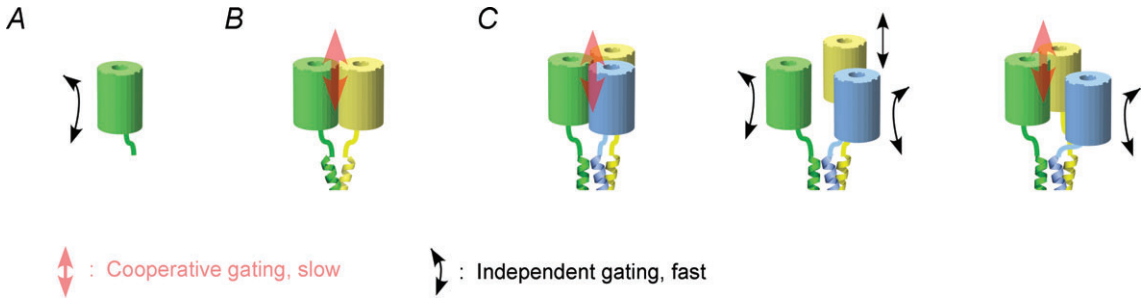

Figure 8. Schematic model of channel gating in the multimers
Alterations of gating kinetics, sigmoidicity in activation and tail current components among WT and mutant channels are assumed to reflect changes in cooperative gating (Fig. 6). Conceivable models, which illustrate the gating of WT and the mutant channels, are presented. *A*, gating model of the monomeric channel (ΔC). The channel gates independently due to a lack of gating partner. *B*, gating model of the dimeric channel (WT). Two channel protomers behave in a cooperative manner, and therefore gating shows slow kinetics. *C*, gating model of the trimeric channel (the I/I or L/L mutant channel). Three possible models are shown. The model of fully cooperative gating, in which three protomers gate with full cooperativity, and the channel gating should show very slow kinetics (left). The model of independent gating, in which three protomers behave fully independently, and gating kinetics should be as fast as that of the monomeric channel (middle). The model of partially cooperative gating, in which two of the channel protomers constitute a unit of cooperative gating and the other one fails to join, consequently showing a mixture of slow and fast gating components (right). The ratio of the slow component based on this model (right) should be 66.7%, if two of three protomers always have a gating cooperativity.

when Hv opens (Gonzalez *et al.* 2010; Tombola *et al.* 2010). This shows up as the sigmoidal and slow activation phase in the dimeric WT channel in comparison with the mono-exponential activation of the monomeric ΔC channel (Figs 6 and 8*A* and *B*) (Gonzalez *et al.* 2010; Musset *et al.* 2010). Concerning the gating in the trimeric channels, it may be predicted that much slower gating kinetics could appear due to the stronger cooperation of gating (Fig. 8*C*, left). However, the trimeric channels showed faster gating kinetics both in activation and deactivation (Fig. 5). The activation kinetics showed less, but clear, sigmoidicity in the trimer mutants, suggesting that the mutants still have some cooperative gating (Fig. 6). Two different components that arise in the trimer channels in deactivation phases (Fig. 7) may reflect that some of the protomers in the mutant channels fail to incorporate into a pair of cooperative channel subunits (Fig 8*C*, right). The rate constant of the slow component of deactivation is in the same range of the rate constant of a single exponential phase of the WT current (Figs. 5 and 7), suggesting that the slow component of deactivation represents the proportion of cooperatively gated protomers in the oligomeric channels. The small amplitude of the slow components (∼20%) (Fig. 7*C*) suggests that, in fact, only a small fraction of channel protomers exert cooperative gating in the trimeric channels. In contrast, the ratio of the slow component predicted based on the model, in which two cooperative protomers and a non-cooperative protomer, was much larger, 66.7%, in the trimeric channel (Fig. 8*C*, right). In addition, activation kinetics of the trimeric mutants did not consist of simple summation of two components (Fig. 6 and Supplementary Fig. S1). These results indicate that the Hv trimer does not behave as a simple combination of a normally functioning dimer and one unpaired protomer. The presence of the two paired subunits, 'dimer within the trimer', could affect the gating of the unpaired protomer, and the extent of this interaction could be different during activation and deactivation. For instance, a strong interaction during activation could delay the opening of the unpaired protomer, resulting in an unclear fast mono-exponential component in the current (Fig. 6 and Supplementary Fig. S1). On the other hand, a weaker interaction during deactivation could explain why the tail current of the trimer shows both the slow component typical of the dimer and the fast component typical of the monomer (Fig. 7).

Our results demonstrate that the I/L sequence pattern of the coiled-coil core in the WT Hv is optimally designed to form dimeric channels with cooperative gating. The cooperativity between the two subunits strengthens the voltage dependence of their proton conductance, which is known to play an important role in regulating NADPH oxidase activity in phagocytes (DeCoursey *et al.* 2003).

References

Acharya A, Rishi V & Vinson C (2006). Stability of 100 homo and heterotypic coiled-coil a-a' pairs for ten amino acids (A, L, I, V, N, K, S, T, E, and R). *Biochemistry* **45**, 11324–11332.

Adams PD, Afonine PV, Bunkoczi G, Chen VB, Davis IW, Echols N, Headd JJ, Hung LW, Kapral GJ, Grosse-Kunstleve RW, McCoy AJ, Moriarty NW, Oeffner R, Read RJ, Richardson DC, Richardson JS, Terwilliger TC & Zwart PH (2010). PHENIX: a comprehensive Python-based system for macromolecular structure solution. *Acta Crystallogr D Biol Crystallogr* **66**, 213–221.

Akey DL, Malashkevich VN & Kim PS (2001). Buried polar residues in coiled-coil interfaces. *Biochemistry* **40**, 6352–6360.

Alber T (1992). Structure of the leucine zipper. *Curr Opin Genet Dev* **2**, 205–210.

Decoursey TE (2003). Voltage-gated proton channels and other proton transfer pathways. *Physiol Rev* **83**, 475–579.

DeCoursey TE, Morgan D & Cherny VV (2003). The voltage dependence of NADPH oxidase reveals why phagocytes need proton channels. *Nature* **422**, 531–534.

Emsley P, Lohkamp B, Scott WG & Cowtan K (2010). Features and development of Coot. *Acta Crystallogr D Biol Crystallogr* **66**, 486–501.

Fujiwara Y & Minor DL Jr (2008). X-ray crystal structure of a TRPM assembly domain reveals an antiparallel four-stranded coiled-coil. *J Mol Biol* **383**, 854–870.

Fujiwara Y, Kurokawa T, Takeshita K, Kobayashi M, Okochi Y, Nakagawa A & Okamura Y (2012). The cytoplasmic coiled-coil mediates cooperative gating temperature sensitivity in the voltage-gated H(+) channel Hv1. *Nat Commun* **3**, 816.

Gonzalez C, Koch HP, Drum BM & Larsson HP (2010). Strong cooperativity between subunits in voltage-gated proton channels. *Nat Struct Mol Biol* **17**, 51–56.

Grigoryan G & Keating AE (2008). Structural specificity in coiled-coil interactions. *Curr Opin Struct Biol* **18**, 477–483.

Harbury PB, Zhang T, Kim PS & Alber T (1993). A switch between two-, three-, and four-stranded coiled coils in GCN4 leucine zipper mutants. *Science* **262**, 1401–1407.

Harbury PB, Kim PS & Alber T (1994). Crystal structure of an isoleucine-zipper trimer. *Nature* **371**, 80–83.

Hartmann MD, Ridderbusch O, Zeth K, Albrecht R, Testa O, Woolfson DN, Sauer G, Dunin-Horkawicz S, Lupas AN & Alvarez BH (2009). A coiled-coil motif that sequesters ions to the hydrophobic core. *Proc Natl Acad Sci U S A* **106**, 16950–16955.

Howard RJ, Clark KA, Holton JM & Minor DL Jr (2007). Structural insight into KCNQ (Kv7) channel assembly and channelopathy. *Neuron* **53**, 663–675.

Kapust RB, Tozser J, Fox JD, Anderson DE, Cherry S, Copeland TD & Waugh DS (2001). Tobacco etch virus protease: mechanism of autolysis and rational design of stable mutants with wild-type catalytic proficiency. *Protein Eng* **14**, 993–1000.

Koch HP, Kurokawa T, Okochi Y, Sasaki M, Okamura Y & Larsson HP (2008). Multimeric nature of voltage-gated proton channels. *Proc Natl Acad Sci U S A* **105**, 9111–9116.

Kuno M, Ando H, Morihata H, Sakai H, Mori H, Sawada M & Oiki S (2009). Temperature dependence of proton permeation through a voltage-gated proton channel. *J Gen Physiol* **134**, 191–205.

Laue TM (1995). Sedimentation equilibrium as thermodynamic tool. *Methods Enzymol* **259**, 427–452.

Lee SY, Letts JA & Mackinnon R (2008). Dimeric subunit stoichiometry of the human voltage-dependent proton channel Hv1. *Proc Natl Acad Sci U S A* **105**, 7692–7695.

Li SJ, Zhao Q, Zhou Q, Unno H, Zhai Y & Sun F (2010). The role and structure of the carboxyl-terminal domain of the human voltage-gated proton channel Hv1. *J Biol Chem* **285**, 12047–12054.

Lishko PV, Botchkina IL, Fedorenko A & Kirichok Y (2010). Acid extrusion from human spermatozoa is mediated by flagellar voltage-gated proton channel. *Cell* **140**, 327–337.

Lupas AN & Gruber M (2005). The structure of alpha-helical coiled coils. *Adv Protein Chem* **70**, 37–78.

Morgan D, Capasso M, Musset B, Cherny VV, Rios E, Dyer MJ & DeCoursey TE (2009). Voltage-gated proton channels maintain pH in human neutrophils during phagocytosis. *Proc Natl Acad Sci U S A* **106**, 18022–18027.

Murshudov GN, Vagin AA & Dodson EJ (1997). Refinement of macromolecular structures by the maximum-likelihood method. *Acta Crystallogr D Biol Crystallogr* **53**, 240–255.

Musset B, Smith SM, Rajan S, Cherny VV, Sujai S, Morgan D & DeCoursey TE (2010). Zinc inhibition of monomeric and dimeric proton channels suggests cooperative gating. *J Physiol* **588**, 1435–1449.

O'Shea EK, Klemm JD, Kim PS & Alber T (1991). X-ray structure of the GCN4 leucine zipper, a two-stranded, parallel coiled coil. *Science* **254**, 539–544.

Okochi Y, Sasaki M, Iwasaki H & Okamura Y (2009). Voltage-gated proton channel is expressed on phagosomes. *Biochem Biophys Res Commun* **382**, 274–279.

Perrakis A, Morris R & Lamzin VS (1999). Automated protein model building combined with iterative structure refinement. *Nat Struct Biol* **6**, 458–463.

Ramsey IS, Moran MM, Chong JA & Clapham DE (2006). A voltage-gated proton-selective channel lacking the pore domain. *Nature* **440**, 1213–1216.

Ramsey IS, Ruchti E, Kaczmarek JS & Clapham DE (2009). Hv1 proton channels are required for high-level NADPH oxidase-dependent superoxide production during the phagocyte respiratory burst. *Proc Natl Acad Sci U S A* **106**, 7642–7647.

Sakata S, Kurokawa T, Norholm MH, Takagi M, Okochi Y, von Heijne G & Okamura Y (2010). Functionality of the voltage-gated proton channel truncated in S4. *Proc Natl Acad Sci U S A* **107**, 2313–2318.

Sasaki M, Takagi M & Okamura Y (2006). A voltage sensor-domain protein is a voltage-gated proton channel. *Science* **312**, 589–592.

Shuart NG, Haitin Y, Camp SS, Black KD & Zagotta WN (2011). Molecular mechanism for 3:1 subunit stoichiometry of rod cyclic nucleotide-gated ion channels. *Nat Commun* **2**, 457.

Strelkov SV & Burkhard P (2002). Analysis of alpha-helical coiled coils with the program TWISTER reveals a structural mechanism for stutter compensation. *J Struct Biol* **137**, 54–64.

Tombola F, Ulbrich MH & Isacoff EY (2008). The voltage-gated proton channel Hv1 has two pores, each controlled by one voltage sensor. *Neuron* **58**, 546–556.

Tombola F, Ulbrich MH, Kohout SC & Isacoff EY (2010). The opening of the two pores of the Hv1 voltage-gated proton channel is tuned by cooperativity. *Nat Struct Mol Biol* **17**, 44–50.

Vagin A & Teplyakov A (2010). Molecular replacement with MOLREP. *Acta Crystallogr D Biol Crystallogr* **66**, 22–25.

Van Petegem F, Clark KA, Chatelain FC & Minor DL Jr (2004). Structure of a complex between a voltage-gated calcium channel beta-subunit and an alpha-subunit domain. *Nature* **429**, 671–675.

Vinson C, Myakishev M, Acharya A, Mir AA, Moll JR & Bonovich M (2002). Classification of human B-ZIP proteins based on dimerization properties. *Mol Cell Biol* **22**, 6321–6335.

Xu Q & Minor DL Jr (2009). Crystal structure of a trimeric form of the K(V)7.1 (KCNQ1) A-domain tail coiled-coil reveals structural plasticity and context dependent changes in a putative coiled-coil trimerization motif. *Protein Sci* **18**, 2100–2114.

Yu Y, Ulbrich MH, Li MH, Buraei Z, Chen XZ, Ong AC, Tong L, Isacoff EY & Yang J (2009). Structural and molecular basis of the assembly of the TRPP2/PKD1 complex. *Proc Natl Acad Sci U S A* **106**, 11558–11563.

Author's present address

T. Kurokawa: Department of Synthetic Chemistry and Biological Chemistry, Graduate School of Engineering, Kyoto University, Japan.

Author contributions

Y.F., H.P.L. and Y.O. designed experiments; Y.F. performed electrophysiological experiments; T.K. performed cross-linking experiments; Y.F. performed protein biochemical experiments; Y.F., K.T. and A.N performed crystallographic analyses; Y.F., H.P.L. and Y.O. wrote the paper. All authors approved the final version.

Acknowledgements

We would like to thank Dr E. Yamashita for data collection and Mrs M. Kobayashi for technical assistance. Diffraction data were collected at the Osaka University beamline BL44XU at SPring-8 (Hyogo) equipped with MX225-HE, which is financially supported by Academia Sinica and National Synchrotron Radiation Research Center (Taiwan, ROC). This work was supported by grants from the Grant-in-Aid for Scientific Research (Y.F. and Y.O.), the Targeted Proteins Research Program (Y.O. and A.N.), and the National Institutes of Health 1R01HL095920-01A2 (H.P.L. and Y.O.).